Title

Oligodendroglial deletion of ESCRT-I component TSG101 causes spongiform encephalopathy

Journal

Biology of the Cell, 108(11)

ISSN

0248-4900

Authors

Walker, Will P
Oehler, Abby
Edinger, Aimee L
et al.

Publication Date

2016-11-01

DOI

10.1111/boc.201600014

Biol. Cell (2016) **108,** 324–337 DOI: 10.1111/boc.201600014

Research article

Oligodendroglial deletion of ESCRT-I component TSG101 causes spongiform encephalopathy

Will P. Walker*, Abby Oehler†, Aimee L. Edinger‡, Kay-Uwe Wagner§ and Teresa M. Gunn*[1]

*McLaughlin Research Institute, Great Falls, MT 59405, USA, †Department of Pathology, Institute for Neurodegenerative Diseases, University of California, San Francisco, CA 94143, USA, ‡Department of Developmental and Cell Biology, University of California, Irvine, CA 92697, USA, and §Eppley Institute for Research in Cancer and Allied Diseases, University of Nebraska Medical Center, Omaha, NE 68198, USA

Background Information. Vacuolation of the central nervous system (CNS) is observed in patients with transmissible spongiform encephalopathy, HIV-related encephalopathy and some inherited diseases, but the underlying cellular mechanisms remain poorly understood. Mice lacking the mahogunin ring finger-1 (MGRN1) E3 ubiquitin ligase develop progressive, widespread spongiform degeneration of the CNS. MGRN1 ubiquitinates and regulates tumour susceptibility gene 101 (TSG101), a central component of the endosomal trafficking machinery. As loss of MGRN1 is predicted to cause partial TSG101 loss-of-function, we hypothesised that CNS vacuolation in *Mgrn1* null mice may be caused by the accumulation of multi-cisternal endosome-like 'class E' vacuolar protein sorting (vps) compartments similar to those observed in *Tsg101*-depleted cells in culture.

Results. To test this hypothesis, *Tsg101* was deleted from mature oligodendroglia *in vivo*. This resulted in severe spongiform encephalopathy, histopathologically similar to that observed in *Mgrn1* null mutant mice but with a more rapid onset. Vacuoles in the brains of *Tsg101*-deleted and *Mgrn1* mutant mice labelled with endosomal markers, consistent with an endosomal origin. Vacuoles in the brains of mice inoculated with Rocky Mountain Laboratory (RML) prions did not label with these markers, indicating a different origin, consistent with previously published studies that indicate RML prions have a primary effect on neurons and cause vacuolation in an MGRN1-independent manner. Oligodendroglial deletion of *Rab7*, which mediates late endosome-to-lysosome trafficking and autophagosome–lysosome fusion, did not cause spongiform change.

Conclusions. Our data suggest that the formation of multi-cisternal 'class E' vps endosomal structures in oligodendroglia leads to vacuolation.

Significance. This work provides the first evidence that disrupting multi-vesicular body formation in oligodendroglia can cause white matter vacuolation and demyelination. HIV is known to hijack the endosomal sorting machinery, suggesting that HIV infection of the CNS may also act through this pathway to cause encephalopathy.

Introduction

Spongiform encephalopathy is a neurodegenerative pathology characterised by large, membrane-bound vacuolar structures (Masters and Richardson, 1978). While considered a hallmark of transmissible spongiform encephalopathies (TSEs) and inherited prion diseases, vacuoles are also associated with certain retroviral infections of the central nervous system (CNS) (including HIV), inherited leukodystrophies, such as Canavan disease, Leigh syndrome or Pelizaeus–Merzbacher disease, and sometimes with

[1]To whom correspondence should be addressed (email: tmg@mri.montana.edu)

Key words: Endosomal sorting complex required for transport, Mahogunin ring finger-1, Spongiform neurodegeneration, Transmissible spongiform encephalopathy, Tumour susceptibility gene 101.

Abbreviations: CHMP2B, charged multi-vesicular body protein 2B; CNS, central nervous system (CNS); ESCRT, endosomal sorting complex required for transport; FTD-3, frontotemporal dementia linked to chromosome 3 (FTD-3); HIVE, HIV-related encephalopathy; IHC, immunohistochemistry; MGRN1, mahogunin ring finger 1; MVB, multi-vesicular body; RAB7, RAS-related GTP-binding protein 7; RML, Rocky Mountain Laboratory; TSE, transmissible spongiform encephalopathy; TSG101, tumour susceptibility gene 101; *vps*, vacuolar protein sorting.

more common forms of neurodegeneration, including Alzheimer's disease (Mancardi et al., 1982; Smith et al., 1987; Artigas et al., 1989; Martinez et al., 1995; Brown and Squier, 1996; Budka, 2003; Gomez-Lucia, 2005; Kumar et al., 2006). The origin of CNS vacuoles remains unclear, although plasma membrane abnormalities and excess aberrant multivesicular bodies (MVBs) noted in ultrastructural studies of TSE suggest that the formation of abnormal configurations of membrane may be involved (Beck et al., 1982; Liberski, 2004; Ersdal et al., 2009).

Endo-lysosomal trafficking regulates lysosome biogenesis and membrane protein signalling and turnover. Canonical endosomal trafficking of membrane proteins involves endosomal sorting complex required for transport (ESCRT) proteins, which recognise ubiquitinated membrane proteins on the surface of endosomes and package them into the intra-lumenal vesicles of incipient MVBs. Mature MVBs then traffic to and fuse with lysosomes, releasing their intra-lumenal cargo into the lysosome for degradation (Henne et al,. 2011; Lee and Gao, 2012). ESCRT proteins are also involved in other cellular processes, including viral budding, cytokinesis, autophagy and cell death. In humans, mutations in the genes encoding the ESCRT-I component VPS37A or the ESCRT-III subunit charged multivesicular body protein 2B (CHMP2B) underlie an autosomal recessive form of complex hereditary spastic paraparesis and a rare familial form of frontotemporal dementia linked to chromosome 3 (FTD-3), respectively (Skibinski et al., 2005; Zivony-Elboum et al., 2012). The brains of FTD-3 patients showed loss of cortical neurons, micro-vacuolation of layer II, gliosis and demyelination with accumulation of ubiquitinated inclusions and the autophagy marker, p62, but not of TAR DNA binding protein (also known as TDP-43) (Holm et al., 2007). Abnormalities in endo-lysosomal trafficking in neurons are generally associated with neuronal degeneration (Skibinski et al., 2005; Parkinson et al., 2006; van der Zee et al., 2008; Wang et al., 2013) and thus are associated with many neurodegenerative disorders, including Alzheimer's, Huntington's and Parkinson's diseases and FTD (Shacka et al., 2008; Kuo et al., 2013). While the consequences of disrupted endosomal trafficking in oligodendroglia have not been explored, this pathway has been implicated in myelin production through the trafficking of myelin proteins (Trajkovic et al., 2006; Kramer-Albers et al., 2007; Winterstein et al., 2008; Stendel et al., 2010; Feldmann et al., 2011; Baron et al., 2015).

A link between disrupted endo-lysosomal trafficking and spongiform neurodegeneration was suggested by the identification of the ESCRT-I protein TSG101 as a substrate of the mahogunin ring finger 1 (MGRN1) ubiquitin ligase (Kim et al., 2007; Jiao et al., 2009b). *Mgrn1*$^{md\text{-}nc/md\text{-}nc}$ (null) mutant mice develop widespread spongiform encephalopathy, predominantly affecting white matter-rich brain regions (He et al., 2003). Vacuoles are first apparent between 6 and 9 months of age and increase in size and number with age. Abnormal TSG101 ubiquitination and solubility and impaired ESCRT-dependent trafficking were observed in the brains of *Mgrn1* null mutant mice well before the appearance of histologically detectable vacuoles (Jiao et al., 2009b), suggesting that TSG101 dysfunction could be the proximal cause of vacuolation. Depletion of TSG101 from yeast or mammalian cells leads to the development of 'class E' vacuolar protein sorting *(vps)* compartments, which are thought to derive from the accumulation of endosomal membranes when normal ESCRT-dependent cargo sorting and endosomal maturation are blocked (Doyotte et al., 2005; Razi and Futter, 2006). Like spongiform vacuoles, these are large, abnormal, progressively accumulating intra-cellular membranous structures, which led us to hypothesise that spongiform vacuoles may be a neurohistopathological manifestation of 'class E' *vps* compartments. To test this, we examined whether loss of TSG101 was sufficient to cause CNS vacuolation. Because conventional *Tsg101* knockout mice are embryonic lethal (Wagner et al., 2003), we used tamoxifen-induced conditional mutagenesis to delete *Tsg101* from oligodendroglia. Our results show that this caused spongiform neurodegeneration similar to that observed in *Mgrn1* null mutant mice, but with a more rapid onset. Vacuoles in the brains of *Tsg101*-deleted and *Mgrn1* null mutant mice labelled for endosomal markers, while those caused by intra-cerebral inoculation of Rocky Mountain Laboratory (RML) prions did not, consistent with our previous work indicating that vacuolation caused by RML prions is MGRN1-independent Silvius et al., 2013. Oligodendroglial deletion of the gene encoding the small GTPase RAS-related GTP-binding protein 7 (RAB7), which mediates late endosomal trafficking and fusion with autophagosomes,

did not cause spongiform change. These results implicate defective MVB formation in the biogenesis of CNS vacuoles.

Results

Deleting *Tsg101* from oligodendroglia causes severe white matter vacuolation

As vacuolation appears first and is most severe in myelin-rich regions of *Mgrn1* null mutant brains (*i.e.* thalamus, cerebellar white matter and brainstem) (He et al., 2003; Jiao et al., 2009a), *Tsg101* conditional knockout mice were mated to *Plp1-cre/ERT* transgenic mice, which express tamoxifen-inducible cre recombinase in oligodendroglia (Doerflinger et al., 2003). Animals were given tamoxifen at 3–4 wk of age. Cre activity in the CNS was assessed at 2 wk post-tamoxifen treatment using the ROSA26 reporter line. Strong X-gal staining was observed in the brainstem (including the pons), cerebellar white matter, corpus collosum and white matter tracts in the thalamus, consistent with previous reports of oligodendroglial-specific expression in the CNS (Doerflinger et al., 2003 and http://cre.jax.org/Plp1ERT/Plp1ERT.html; data not shown). Deletion of *Tsg101* was verified by PCR on DNA isolated from dissected regions of the CNS of tamoxifen-treated $Tsg101^{fl/fl}$;*Plp1-cre/ERT*+ mice (Figure 1A-B). Some background recombinase activity was detected in the thalamus, hindbrain and spinal cord of $Tsg101^{fl/fl}$; *Plp1-cre/ERT*+ mice treated with vehicle alone (Figure 1B). The Plp1-creERT transgene was recently reported to drive a similar, modest level of gene recombination in the absence of tamoxifen treatment in another study as well (Traka et al., 2016). TSG101 protein levels in the brains of tamoxifen-treated $Tsg101^{fl/fl}$; *Plp1-cre/ERT*+ were significantly reduced, being 61% of tamoxifen-treated $Tsg101^{fl/fl}$; *Plp1-cre/ERT*- controls ($P = 0.02$; Figure 1C).

Within 2 wk of tamoxifen treatment, all $Tsg101^{fl/fl}$; *Plp1-cre/ERT*+ mice ($n>25$) exhibited weakness, kyphotic posture, action tremor and ataxic gait. Histopathological evaluation of their brains 2 wk after tamoxifen treatment revealed extensive vacuolation in white matter of the pons, cerebellum and thalamus (Figures 1D–1G). Mild, progressive vacuolation was observed in all uninjected ($n>15$) and control injected (sunflower oil, $n>12$) $Tsg101^{fl/fl}$; *Plp1-cre/ERT*+ mice (Figure 2A), most likely due to the background activity that we observed for the *Plp1-cre/ERT* transgene (Figure 1B). These untreated $Tsg101^{fl/fl}$; *Plp1-cre/ERT*+ mice also developed a tremor and had significantly reduced body weight by 8 wk of age (Figure 2B). No CNS vacuolation or tremor was observed in $Tsg101^{fl/fl}$ mice that did not carry the cre transgene or in any $Tsg101^{fl/+}$ animals. Vacuolation in the brains of tamoxifen-treated $Tsg101^{fl/fl}$; *Plp1-cre/ERT*+ mice was associated with severe gliosis, as indicated by GFAP immunoreactivity (Figure 3A). Inclusions of ubiquitinated proteins accumulated in the cytoplasm of oligodendrocytes in affected brain regions, as well as on the limiting membranes of spongiform vacuoles (Figures 3B and 4A–4B). In vacuolated brain regions, cells staining positive for the oligodendrocyte markers CC-1 and sex determining region Y-box 10 (SOX10) showed increased immunoreactivity for the autophagy marker, p62, but vacuoles themselves only occasionally showed small punctae of p62 staining on their limiting membranes (Figures 3C and 4C–4D). Vacuoles do not appear to be caused by cell death since they were observed in the absence of activated caspase-3 (CC3) in the thalamus (Figure 3D), and the most heavily vacuolated regions of the pons and cerebellum showed CC3 staining in association with both vacuoles and unvacuolated cells (Figures 3D and 4E–4F).

Vacuolation was most severe in MBP-rich white matter tracts (Figures 4I–4K). Vacuoles were often observed within cells expressing SOX10 (Figures 4A, 4C and 4E), consistent with their having a cell autonomous origin. The response of oligodendrocytes to loss of *Tsg101* varied, even within a brain region, as some SOX10-positive cells were associated with vacuoles and/or immunoreactivity for ubiquitin, p62 or CC3, while others appeared histologically normal (Figures 4A–4F). CC3 accumulation was not observed in neurons or astrocytes (Figures 4G–4H), indicating that disrupted endosomal trafficking in oligodendroglia causes cell autonomous defects and does not cause apoptosis of neighbouring cells. Loss of *Tsg101* appeared to have a progressive effect on oligodendroglial function, as assessed by Luxol fast blue staining of myelin lipoproteins. While similar levels of staining were observed in $Tsg101^{fl/fl}$; *Plp1-cre/ERT* and $Tsg101^{fl/+}$; *Plp1-cre/ERT* brains 2 wk after tamoxifen treatment, reduced staining was observed in

Figure 1 | Oligodendroglial deletion of *Tsg101* causes spongiform encephalopathy

(**A**) Schematic of *Tsg101* floxed and null alleles showing locations of genotyping primers. Primers floxedF and floxedR amplify a segment of the PGK-neo cassette, present only in the floxed allele, while nullF and nullR amplify across the loxP site (triangle) remaining when the PGK-neo cassette and exon1 are deleted by cre-mediated recombination. Although the null primers are present in the floxed allele, they are too far apart to generate a product using standard PCR conditions. (**B**) *Tsg101* deletion by Plp1-cre/ERT was detected using allele-specific PCR to amplify the $Tsg101^{fl}$ allele (top panels) or the $Tsg101^{null}$ allele (bottom panels) from DNA isolated from dissected tissues of Plp1-cre/ERT transgenic and non-transgenic $Tsg101^{fl/+}$ animals 2 wk after administration of tamoxifen or vehicle control. Results shown are representative of four independent samples. Observation of the null allele in some vehicle only samples is consistent with a low level of background (uninduced) cre activity. (**C**) Western blots of three independent $Tsg101^{fl/fl}$; Plp1-cre/ERT brain lysates show 39% reduction in TSG101 protein levels in cre(+) brain tissues 2 wk after the initiation of tamoxifen treatment. Blots were quantified using ImageJ, with TSG101 levels normalised against GAPDH. **(D–E)** Images from C57BL/6J coronal mouse brain atlas (www.mbl.org/atlas170/atlas170_frame.html) with labelled boxes indicating approximate location within the thalamus, cerebellum and pons represented in F and G. **(F)** Low-magnification views of hematoxylin and eosin (H&E)-stained sections of thalamus (top), pons (middle) and cerebellum (bottom) of tamoxifen-treated control ($Tsg101^{fl/fl}$; *Plp1-cre/ERT*- and $Tsg101^{fl/+}$; *Plp1-cre/ERT*+) and *Tsg101*-ablated ($Tsg101^{fl/fl}$; *Plp1-cre/ERT*+) mice 2 wk after the initiation of tamoxifen treatment. All panels in F are shown at the same magnification. Scale bar: 500 μm. **(G)** High-magnification views of thalamus, pons and cerebellum from tamoxifen-treated control and *Tsg101*-ablated mice 2 wk after the initiation of tamoxifen treatment. All panels in G are shown at same magnification. Scale bar: 50 μm.

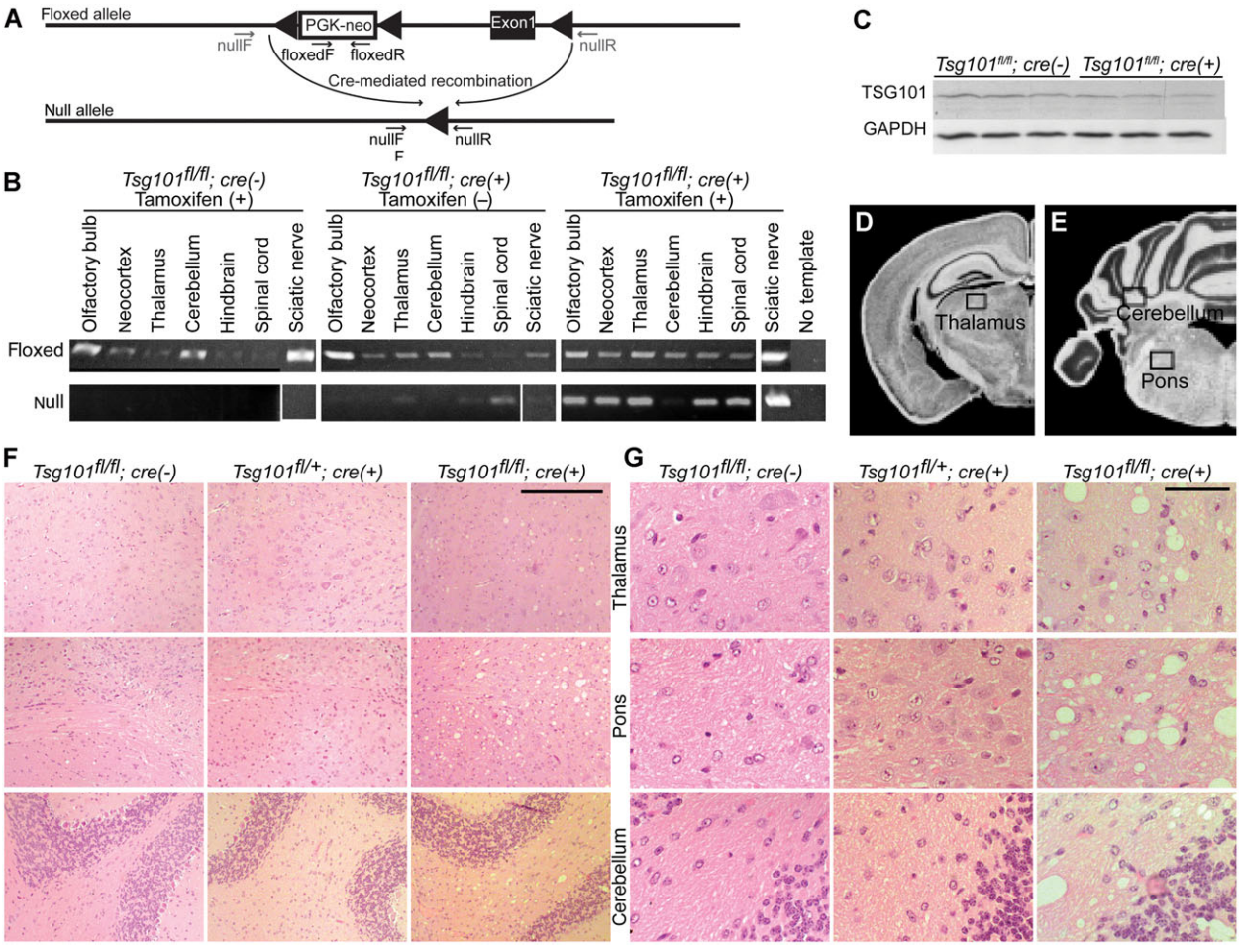

Figure 2 | Phenotypes associated with uninduced deletion of *Tsg101* from oligodendroglia

(**A**) Low background levels of cre expression in *Tsg101$^{fl/fl}$; Plp1-cre/ERT+* mice not given tamoxifen result in progressive spongiform change, apparent by 6 wk of age. Scale bars: 10 μm. **(B)** *Tsg101$^{fl/fl}$; Plp1-cre/ERT+* mice not given tamoxifen also show a significant reduction in body weight relative to all control genotypes, starting by 8 wk of age and persisting to at least 12 months of age.

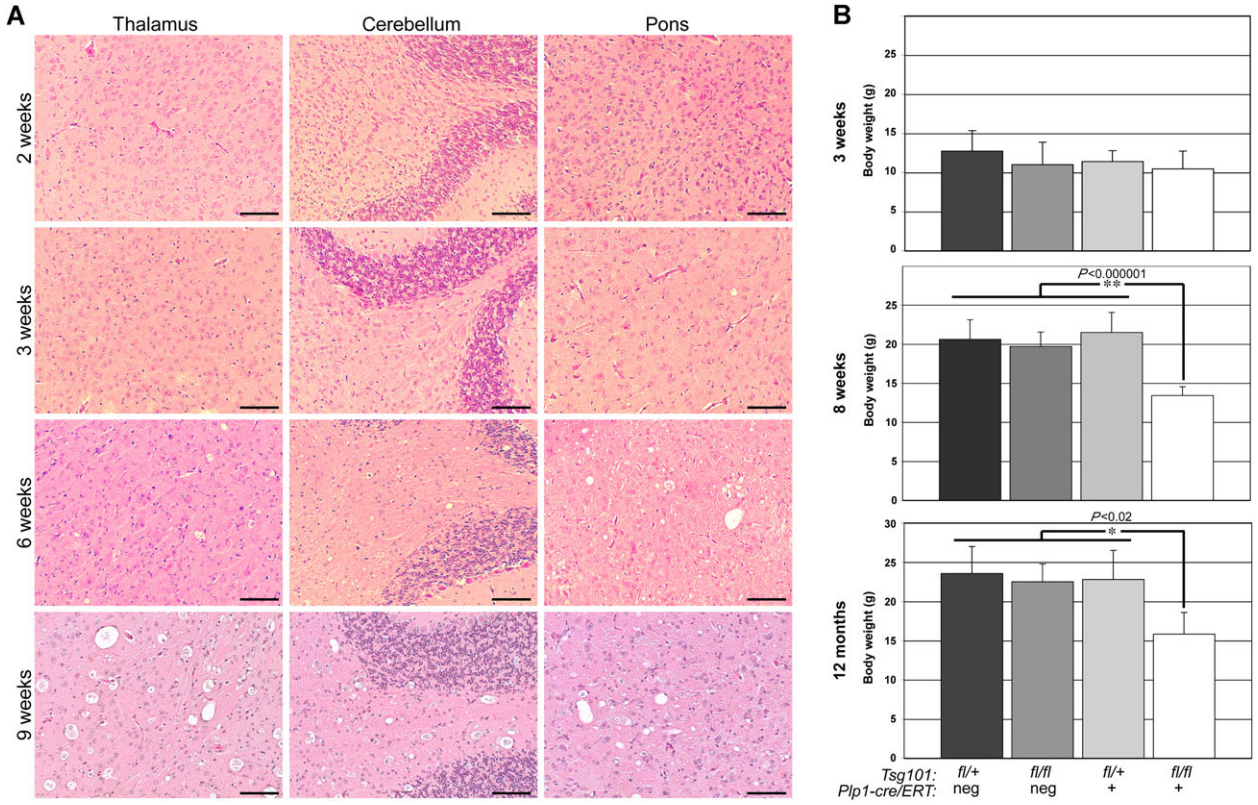

Tsg101$^{fl/fl}$;Plp1-cre/ERT brains 1 wk later (Figure 4K), indicating that loss of TSG101 disrupts myelin homeostasis.

Vacuoles caused by loss of *Tsg101 or Mgrn1* label for endosomal markers

In mammalian cells in culture, siRNA depletion of endogenous *TSG101* inhibits MVB formation and leads to the accumulation of multi-cisternal tubular structures that label for the early endosome marker, EEA1 (Razi and Futter, 2006). Recycling to the cell surface is also reduced, with MVB-dependent pathways most affected (Doyotte et al., 2005). To test the hypothesis that vacuoles are an oligodendroglial manifestation of 'class E' *vps* compartments, IHC was performed for the following endosomal markers: EEA1 and RAB5 (early endosomes), RAB7 (late endosomes/lysosomes) and RAB11 (recycling endosomes). The limiting membrane of over 50% of thalamic vacuoles in *Tsg101$^{fl/fl}$;Plp1-cre/ERT* brains labelled for EEA1, RAB7 and RAB11, while a smaller proportion labelled for RAB5 (Figure 5). Labelling was also observed on the 'membranous structures' often observed within vacuoles. No vacuolar labelling was seen with secondary antibody alone or with isotype-matched antibodies against non-endosomal proteins (data not shown). The neurohistopathology associated with deleting *Tsg101* from oligodendroglia was very similar to that observed in *Mgrn1* null mutants, including the anatomical distribution of vacuoles. In both cases, spongiform change occurred first and was most severe in the brainstem, cerebellum and thalamus, and a similar proportion of thalamic vacuoles showed positive staining for

Figure 3 | Immunohistochemical phenotypes observed 2 wk after oligodendroglial deletion of *Tsg101*
(**A**) Vacuolation in the brains of *Tsg101*-ablated (*Tsg101*$^{fl/fl}$; *Plp1-cre/ERT+*) mice is associated with astrogliosis, as indicated by immunoreactivity for GFAP (brown staining). Scale bars: 20 μm. **(B)** The FK2 antibody, which detects ubiquitinated proteins, reveals ubiquitinated protein inclusions (brown staining) in the thalamus, cerebellum and pons of *Tsg101*-ablated mice, but not in controls (*Tsg101*$^{fl/fl}$; *Plp1-cre/ERT-* or *Tsg101*$^{fl/+}$; *Plp1-cre/ERT+*). Boxed regions in centre panels are shown below at higher magnification. Arrowheads indicate some of the inclusions. Scale bars: 25 μm. **(C)** Cells with elevated levels of the autophagy marker, p62 (brown staining in left and middle panel), are observed adjacent to vacuoles in the thalamus of *Tsg101*-ablated animals but not in control brains. Right panel: dual staining for p62 (green) with the oligodendrocyte marker, CC-1 (red), indicates that these p62-positive cells are oligodendrocytes. **(D)** Cells with strong cytoplasmic labelling for cleaved caspase-3, which marks apoptotic cells, are prominent in the cerebellum and pons of *Tsg101*-ablated animals but not in control brains. The thalamus of *Tsg101*-ablated mice did not show elevated cleaved caspase-3 staining. Boxed regions in centre panels are shown below at higher magnification, with arrowheads indicating cells with strong CC3 signal. Scale bars: 25 μm.

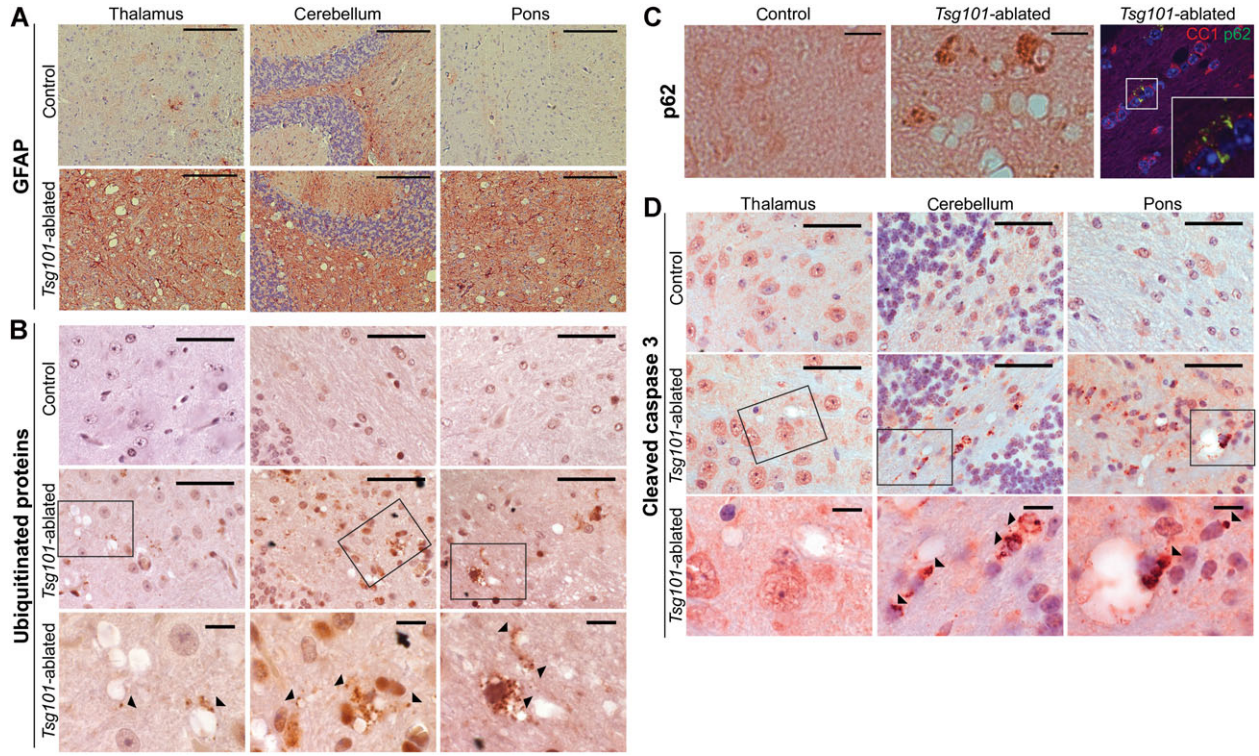

EEA1, RAB5, RAB11 and RAB7 (Figure 5). One difference between vacuoles in *Tsg101*-ablated and *Mgrn1* null mutant brains was that the latter were not associated with ubiquitinated protein inclusions or obvious accumulation of p62 (data not shown), suggesting that those phenotypes may require MGRN1-mediated ubiquitination.

Vacuoles caused by RML prions do not label for endosomal markers

To test whether disrupted endosomal trafficking might be a shared pathogenic mechanism underlying spongiform neurodegeneration associated with other diseases, we tested whether vacuoles in the brains of sick FVB mice inoculated with RML prions label for endosomal markers. Moderate vacuolation was readily apparent in the thalamus and other brain regions of these mice, but IHC for EEA1, RAB7 and RAB11 revealed no labelling of vacuoles (Figure 5). This suggests that vacuoles associated with RML infection likely arise through a TSG101- and MGRN1-independent mechanism that does not involve the accumulation of endosomal compartments. These data also demonstrate that endosomal labelling

Figure 4 | Thalamic vacuoles caused by oligodendroglial deletion of *Tsg101* are cell autonomous and associated with progressive demyelination

(**A–F**) Ubiquitinated proteins (brown staining in A, B), the autophagy adapter p62 (brown staining in C, D) and the apoptosis marker cleaved caspase-3 (CC3, brown staining in E, F) accumulate within SOX10-positive oligodendrocytes (blue staining) in the brains of *Tsg101*-ablated mice, although not all oligodendrocytes are affected. Scale bars: 20 μm. **(G–H)** Oligodendroglial deletion of *Tsg101* does not cause apoptosis (as judged by CC3 staining, in green) in neurons (marked by NeuN, red) or astrocytes (marked by GFAP, red). Nuclei are stained blue. Scale bars: 10 μm. **(I–K)** Vacuoles in the cerebellum (I), pons (J) and thalamus (K) of *Tsg101*-ablated mice (*Tsg101*$^{fl/fl}$; *Plp1-cre/ERT+*) are predominantly located within white matter tracts (indicated by MBP immunoreactivity, blue staining). Scale bars: 250 μm. **(L)** Luxol fast blue staining of myelin proteins was performed on brain sections from tamoxifen-treated *Tsg101*-ablated (*Tsg101*$^{fl/fl}$; *Plp1-cre/ERT+*) and control (*Tsg101*$^{fl/+}$; *Plp1-cre/ERT+*) mice. Similar levels of staining were observed 14 days after initiation of tamoxifen treatment (top panels), but staining was greatly reduced in *Tsg101*-ablated mice relative to controls by 22 days post-treatment (bottom panels).

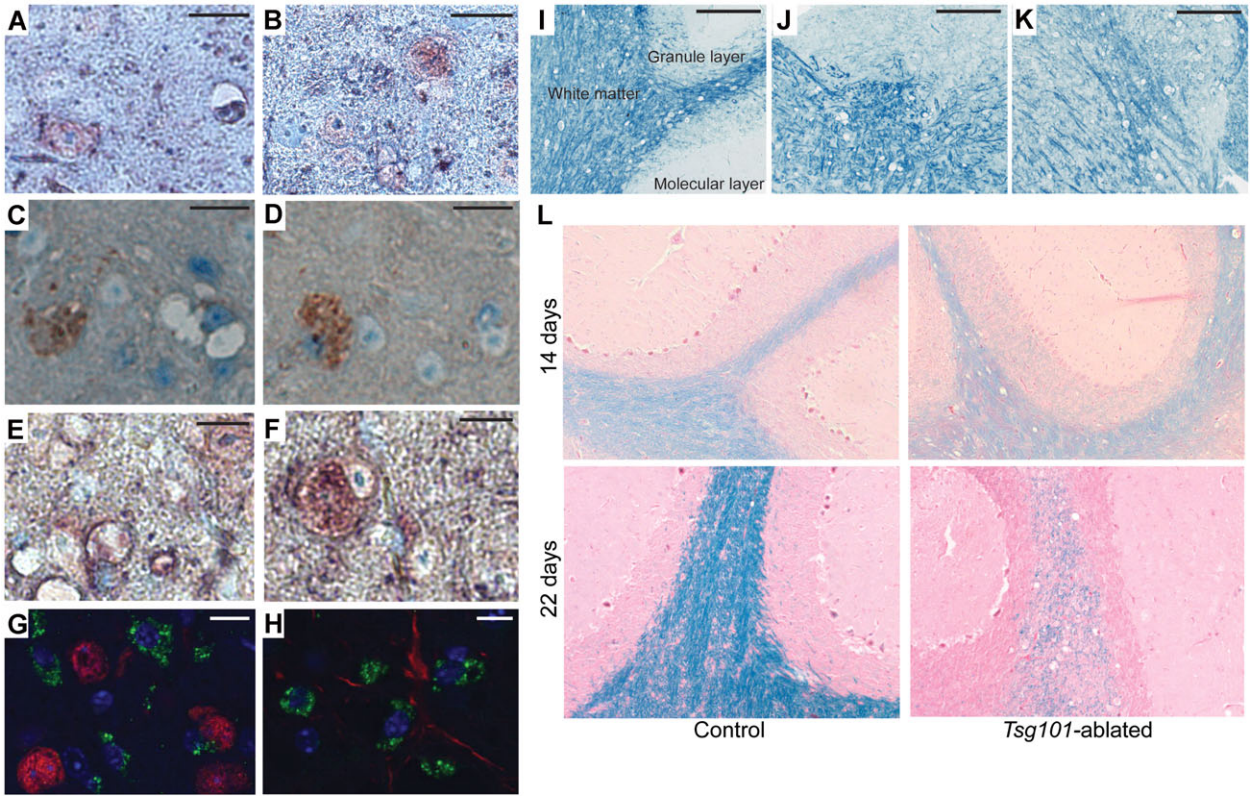

of vacuoles in the brains of *Tsg101*-ablated and *Mgrn1* null mice is not an artefact associated with the presence of vacuoles.

Oligodendroglial deletion of Rab7 does not cause spongiform change

TSG101 is required for the sorting of ubiquitinated receptors into MVBs, which results in downregulation of signalling proteins. MVBs can subsequently traffic their contents to lysosomes, autophagosomes, the recycling pathway or the plasma membrane. To test whether disrupting lysosomal or autophagosomal trafficking in oligodendroglia downstream of TSG101 causes vacuolation, we ablated the gene encoding the small GTPase RAB7, which mediates late endosomal trafficking and autophagosome–lysosome fusion. *Rab7* conditional knockout mice were mated to Plp1-cre/ERT transgenic mice and treated with tamoxifen or oil at 2–4 months of age. *Rab7* deletion was verified by PCR on

Figure 5 | Endosomal markers accumulate on vacuoles caused by oligodendroglial deletion of *Tsg101* or the absence of *Mgrn1* but not by RML prions

(A–D) IHC for the early endosome makers EEA1 (A) and RAB5 (B), late endosome marker RAB7 (C) and recycling endosome marker RAB11 (D) reveals increased expression in association with vacuoles (arrowheads) in the thalamus of *Tsg101*-ablated (tamoxifen-treated *Tsg101*$^{fl/fl}$; *Plp1-cre/ERT+*) and *Mgrn1* null mutant mice but not in RML inoculated mice. ND: no data. Images in A and D are overexposed to facilitate visualisation of vacuoles. Scale bars: 25 μm.

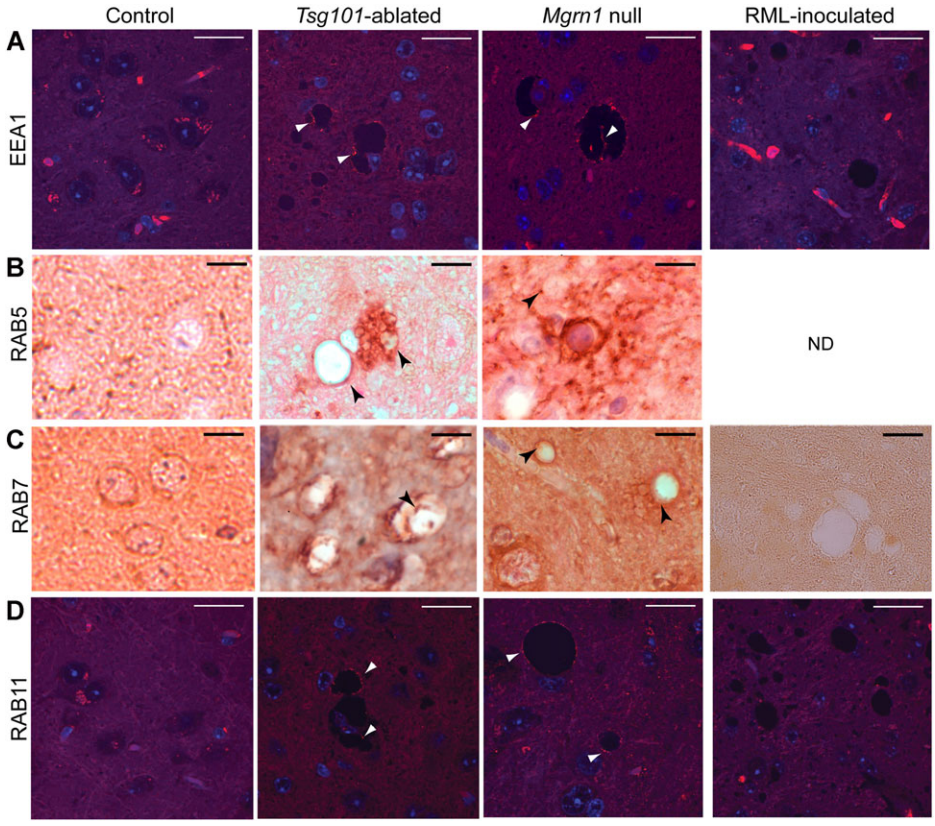

DNA isolated from the cerebellum of tamoxifen-treated *Rab7*$^{fl/fl}$*;Plp1-cre/ERT+* and control mice (Figure 6A). Histological examination of brains from *Rab7*$^{fl/fl}$*;Plp1-cre/ERT+* and control mice 2 wk and 6 and 12 months after tamoxifen or oil injections revealed no significant vacuolation or other histopathological abnormalities (Figure 6B–6D and data not shown), nor did the animals show any overt signs of neurological dysfunction.

Discussion

Loss of *Tsg101* from oligodendroglia caused spongiform vacuolation and demyelination, associated with gliosis and accumulation of ubiquitinated proteins, p62 and endosomal markers including EEA1, RAB5, RAB11 and RAB7. Caspase-mediated apoptosis was triggered in many cells lacking TSG101, with some subpopulations of oligodendroglia appearing to respond more rapidly than others. The brains of FTD-3 patients with mutations in CHMP2B show many similar changes, including demyelination, gliosis and accumulation of ubiquitinated inclusions and p62, suggesting that loss of ESCRT-I function has similar effects to loss of ESCRT-III. It has been suggested that mutations in *CHMP2B* cause FTD-3 because they disrupt late endosome-lysosome fusion and autophagy (Lee and Gao, 2009; Urwin et al., 2010; Clayton et al., 2015; Krasniak and Ahmad, 2016), but our study shows that loss of RAB7,

Figure 6 | Oligodendroglial deletion of *Rab7*

(**A**) *Rab7* deletion by Plp1-cre/ERT was confirmed using PCR to detect the cre transgene (top panel) and the *Rab7* wildtype, floxed and null alleles (bottom panels) from DNA isolated from cerebella dissected from wildtype mice, Plp1-cre/ERT transgenic (cre+) $Rab7^{fl/+}$ and $Rab7^{fl/fl}$ mice, and non-transgenic (cre-) $Rab7^{fl/fl}$ animals 6 months after administration of tamoxifen. *Rab7* wt/floxed PCR detects the wildtype (smaller band) and floxed (larger band) alleles. Consistent with *Rab7* being deleted in oligodendrocytes upon tamoxifen treatment, only the floxed and null alleles are detected in $Rab7^{fl/fl}$; *Plp1-cre/ERT*+ cerebella, while all three alleles (wildtype, floxed and null) are all detected in $Rab7^{fl/+}$; *Plp1-cre/ERT*+ cerebella. **(B–D)** H&E-stained sections of thalamus (A), pons (B) and cerebellum (C) of $Rab7^{fl/fl}$; *Plp1-cre/ERT*+ mice 12 months after tamoxifen treatment. Images in the two left columns of Figure 1E can be compared as controls. Scale bars: 50 μm.

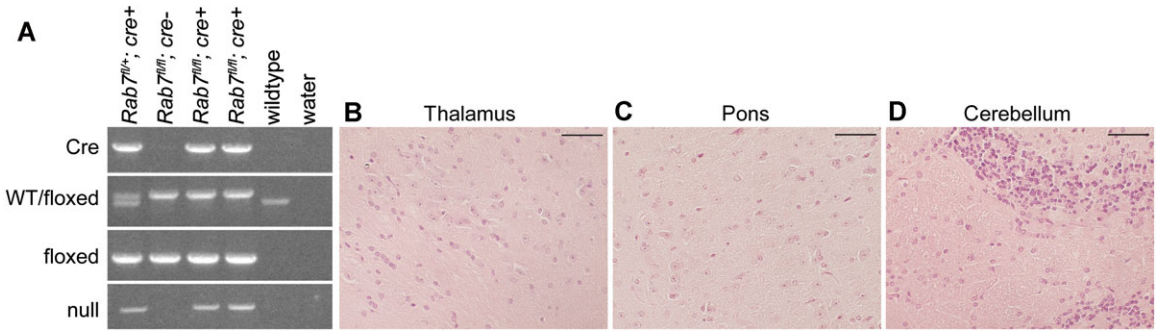

which mediates late endosome-to-lysosome trafficking and autophagosome–lysosome fusion events, does not cause vacuolation.

Why does deleting TSG101 from oligodendroglia cause vacuolation, while loss of RAB7 does not? A clue may come from the effect that knocking each gene down in cultured mammalian cells has on endosomal compartments. Depletion of *Rab7* led to the accumulation of enlarged MVBs/late endosomes and a reduction in the size and number of lysosomes, but multi-cisternal endosomes were not observed (Vanlandingham and Ceresa, 2009). Depletion of *Tsg101*, on the other hand, led to the accumulation of multi-cisternal, EEA1-positive tubular structures as well as enlarged vacuolar compartments similar in appearance to MVBs (Doyotte et al., 2005; Razi and Futter, 2006). The labelling of spongiform vacuoles in *Tsg101*-deleted and *Mgrn1* null brains with antibodies against endosomal proteins strongly suggests that they arise due to a block in ESCRT-mediated MVB formation, but vacuoles do not appear to simply represent the accumulation of 'any' endosomal compartment since deletion of *Rab7* did not cause spongiform change. We propose that vacuoles are a histopathological manifestation of the multi-cisternal 'class E' *vps* compartments that accumulate when the formation of intra-luminal vesicles at the MVB is disrupted. Consistent with this hypothesis, depleting mammalian cells of the ESCRT-0 protein hepatocyte growth factor (HGF)-regulated tyrosine kinase substrate (HGS, also known as hepatocyte growth factor receptor substrate, HRS) did not induce tubular or multi-cisternal early endosomal structures (Razi and Futter, 2006), and mice homozygous for a *Hgs* loss-of-function allele do not develop spongiform neurodegeneration (Watson et al., 2015).

Deleting *Tsg101* from oligodendroglia appears to affect multiple pathways within the endosomal system, based on the accumulation of early, recycling and late endosomal markers on vacuoles. Oligodendrocytes may be especially vulnerable to disrupted membrane trafficking because they generate and traffic large amounts of intra-cellular membrane for myelin production. The progressive demyelination associated with oligodendroglial deletion of *Tsg101* might be a result of sequestration of membrane components on accumulating endosomal compartments, combined with disrupted trafficking of myelin components such as proteolipid protein, myelin-associated glycoprotein and myelin oligodendrocyte protein. These proteins normally traffic through the endosomal system to the plasma membrane and are

released *via* either exosomes or recycling endosomes (Simons et al., 2002; Trajkovic et al., 2006; Winterstein et al., 2008; Chen et al., 2012).

Our results indicate that *Tsg101* dysfunction in oligodendroglia is sufficient to cause spongiform encephalopathy similar to that seen in *Mgrn1* mutant mice, TSEs, HIV-encephalopathy and mitochondrial encephalopathies. Taken together with recent evidence for the regulation of TSG101 by MGRN1, this suggests that impaired TSG101 function in oligodendroglia may be the proximal cause of vacuolation in *Mgrn1* mutants. The later onset of vacuolation in *Mgrn1* mutants (6–9 months of age) may reflect the fact that loss of MGRN1 causes only a partial loss of TSG101 function (Jiao et al., 2009b). The failure to observe ubiquitinated protein inclusions or accumulation of cleaved caspase-3 in *Mgrn1* null brains was not surprising as we previously demonstrated mitochondrial dysfunction and significantly reduced ATP levels in the brains of these animals (Sun et al., 2007). ATP-dependent processes such as ubiquitination and apoptosis would therefore be impaired in the brains of *Mgrn1* null mutant mice. As the effect of loss of MGRN1 on mitochondrial function and ATP levels is most likely TSG101-independent, ubiquitination and apoptosis would not be affected when *Tsg101* is ablated. This suggests that vacuolation is not caused by the accumulation of ubiquitinated protein inclusions or induction of apoptosis, but that these are secondary effects in the brains of *Tsg101*-deleted mice.

Endo-lysosomal trafficking, exosomal secretion and autophagy have been implicated in prion propagation and degradation (Fevrier et al., 2004; Heiseke et al., 2010; Arellano-Anaya et al., 2015), and elevated levels of RAB5 and lysosomal markers cathepsin-B and –D, as well as ubiquitin and p62-positive inclusions, have been noted in neurons in human sporadic and inherited Creutzfeldt–Jakob disease brains (Kovacs et al., 2007; Kovacs et al., 2012). Our examination of vacuolated brain regions in sick mice following inoculation with RML prions did not detect labelling of vacuoles with endosomal markers, but this is perhaps not surprising as the expression pattern of the prion protein and predominance of vacuoles in gray matter in TSE suggest that vacuoles associated with prion diseases have a neuronal origin. Different cellular origins of vacuoles in *Mgrn1* null mutant mice and TSE are consistent with our previous work, which demonstrated that spongiform change and other phenotypes associated with RML prion inoculation were independent of MGRN1 (Silvius et al., 2013). These observations suggest that not all CNS vacuoles share a common cellular origin, although disrupted endo-lysosomal trafficking may be a shared pathway in oligodendrocytes and neurons since mice with mutations that disrupt phosphoinositide-mediated control of endosomal sorting and homeostasis in neurons (*i.e.* *Fig* 4^{plt1}, *Vac14*^{ingls} and *Pikfyve*$^{Gt(AT0926)Wtsi}$) develop spongiform neurodegeneration (Chow et al., 2007; Zhang et al., 2007; Jin et al., 2008; Zolov et al., 2012).

It is intriguing that HIV infection can lead to CNS vacuolation (HIV-related encephalopathy [HIVE]), since HIV-1 GAG has been shown to bind TSG101 and recruit it and the ESCRT machinery to the plasma membrane for viral budding (Mazze and Degreve, 2006; Bleck et al., 2014). This is expected to cause a functional depletion of TSG101 in the endosomal sorting pathway and, in fact, expression of HIV-1 GAG in HEK293T cells disrupted epidermal growth factor receptor (EGFR) downregulation and signalling in a manner similar to that observed when TSG101 was depleted by siRNA knockdown (Valiathan and Resh, 2004). Furthermore, transgenic expression of the HIV-1 genome under control of the oligodendrocyte-specific MBP promoter was sufficient to cause progressive vacuolar myelopathy in mice (Goudreau et al., 1996). Together, these observations suggest that disrupted endosomal trafficking in oligodendroglia should be investigated as a possible pathogenic mechanism – and potential therapeutic target – of spongiform encephalopathy in HIVE.

Materials and methods

Mice

Animals were housed under standard conditions in the Animal Resource Center at the McLaughlin Research Institute. *Tsg101*$^{tm1\text{-}Kuw}$ (*Tsg101*^{fl}) conditional knockout mice, which were created and are maintained on a 129/SvJ genetic background, have been described previously (Wagner et al., 2003). As this allele has loxP sites 3 kb upstream and 230 bp downstream of the first coding exon of *Tsg101*, cre recombinase excises the proximal promoter region and first exon of *Tsg101*, resulting in a null allele. Generation of B6.129(Cg)-*Rab7*$^{tm1.1Ale}$ (*Rab7*^{fl}) conditional knockout mice was described previously (Roy et al., 2013). *Tsg101*$^{fl/fl}$ and *Rab7*$^{fl/fl}$ mice were crossed to the tamoxifen-inducible cre transgenic line B6.Cg-Tg(Plp1-cre/ERT)3Pop/J (referred to as Plp1-cre/ERT), which expresses

cre/ERT in oligodendroglia (Doerflinger et al., 2003), and were obtained from the Jackson Laboratory (stock #005975). Cre-positive F1's were backcrossed to *Tsg101*$^{fl/fl}$ or *Rab7*$^{fl/fl}$ animals to produce *fl/fl* and *fl*/+mice segregating for the Plp1-cre/ERT transgene. B6;129S4 Gt(ROSA)26Sor^{tm1Sor}/J is a β-galactosidase reporter strain (*ROSA26*), initially described by Soriano (1999). They were originally obtained from the Jackson Laboratory (#003309) and maintained in-house. Paraffin sections of brains from clinically scrapie-ill FVB mice inoculated intra-cerebrally at approximately 60 days of age with RML prions (10% brain homogenate from clinically scrapie-ill RML-infected CD-1 mice) were generated from formalin-fixed samples archived from a previous study performed in the laboratory of Dr. Stephen DeArmond at the University of California, San Francisco (UCSF). All animal procedures adhered to Association for Assessment and Accreditation of Laboratory Animal Care guidelines and were approved by the Institutional Animal Care and Use Committees of the McLaughlin Research Institute and UCSF.

Genotyping

Animals were genotyped using PCR. *Tsg101* genotyping primers were: *Tsg101*^{wt}*:* GTTCGCTGAAGTAGAGCAGCCAG and CATTTCTGGAGTCCGATGCGCAG; *Tsg101*^{fl}*:* AGAGGCTATTCGGCTATGACTG and TTCGTCCAGATCATCCTGATC; *Tsg101*^{null}*:* GATGGTCATACCTGGTTAGAAAGC and CATTTCTGGAGTCCGATGCGCAG. *Rab7* genotyping primers were CTCACTCACTCCTAAATGG and TTAGGCTGTATGTATGTGC for the wildtype and floxed alleles and GGGCTGCAGGAATTCGGATAAC and CATGGTAACAAGTCTGTCGTCC for the null allele (Roy et al., 2013). Plp1-cre/ERT transgene genotyping primers were TGCTGTTTCACTGGTTATGCGG and TTGCCCCTGTTTCACTATCCAG. The ROSA26 reporter transgene was detected using the common forward primer AAAGTCGCTCTGAGTTGTTAT and reverse primers GGAGCGGGAGAAATGGATATG (wt) and GCGAAGAGTTTGTCCTCAACC (ROSA+).

Activation and verification of cre recombinase activity

Tsg101 or *Rab7* ablation was induced by twice-daily intraperitoneal injection of 0.025 mg tamoxifen (Sigma) per kg of body weight for 3 consecutive days. To minimise confounding effects of uninduced activity of the Plp1-cre/ERT recombinase in the *Tsg101* cross, animals were given tamoxifen at 3–4 wk of age. For the *Rab7* cross, animals were treated at 2–4 months of age. Tamoxifen was dissolved to 5 μg/ml in a 1:9 mixture of absolute ethanol and pharmacological grade sunflower oil (Sigma). Control animals received injections of the 1:9 ethanol/oil vehicle mixture without tamoxifen. As *Tsg101* deletion caused weight loss, loss of ≥20% of initial body weight was used as an endpoint criterion.

The expression pattern of the Plp1-cre/ERT transgene in the CNS was verified using ROSA26 reporter mice to examine tamoxifen-induced cre-mediated activation of the β-galactosidase reporter gene. Coronal brain slices were incubated for up to 8 h in X-gal staining solution (5 mM EGTA, 2 mM $MgCl_2$, 0.01% sodium deoxycholate, 10 mM potassium ferricyanide, 10 mM potassium ferrocyanide, 0.02% Triton X-100 and 0.5 mg/ml 5-bromo-4-chloro-3-indolyl-b-D-galactopyranoside [X-gal] in 1x PBS) as described (Erdmann et al., 2007). Cre recombinase-mediated deletion of the floxed *Tsg101* or *Rab7* sequence was verified by PCR using the genotyping primers described above and a template of 10 ng genomic DNA isolated from dissected brain regions and sciatic nerve of vehicle- and tamoxifen-injected animals (2 wk post-treatment), as well as from brains of Plp1-cre/ERT negative animals as a further negative control. Reduction of TSG101 protein levels was confirmed by immunoblotting brain lysates isolated 2 wk after tamoxifen treatment, using rabbit anti-TSG101 (ProteinTech Group 14497-1-AP) and mouse anti-GAPDH (Abcam ab9482) as a loading control. Lysates were prepared by homogenising brains in solubilisation buffer (50 mM Tris-HCl pH 8.0, 1 mM EDTA and 1% Igepal CA-630) containing Complete protease inhibitor cocktail (Roche). Blots were imaged using ECL Plus chemiluminescent substrate (Pierce) and quantified using ImageJ. Briefly, after selecting each band, intensity histograms were generated and their areas were measured. For each sample, TSG101 band intensity was normalised against GAPDH intensity prior to statistical analysis.

Histology

Brains were fixed in formalin, processed for histology by standard methods and embedded in paraffin. Experimental and control brains were processed in each batch, with care taken to avoid long exposure to 70% ethanol as this is known to cause artefactual vacuolation in rodent nervous tissue (Wells and Wells, 1989). Paraffin-embedded brains were sectioned at 5 or 8 μm and stained with hematoxylin and eosin or subjected to immunohistochemistry (IHC). The brains of at least five animals were examined for each genotype/treatment combination, except prion inoculated mice (n = 2–4). Unless stated otherwise, data are shown for *Tsg101*$^{fl/fl}$*; Plp1-cre/ERT* brains collected 2 wk after tamoxifen treatment. IHC was performed on paraffin sections pre-treated for antigen retrieval using 10 mM sodium citrate (pH 6.0, 100°C, 10 min). Primary antibodies used were: rabbit anti-cleaved caspase-3 (Trevigen 2305-PC), rabbit anti-GFAP (ProteinTech Group 16825-1-AP), rat anti-GFAP (Invitrogen 130300), mouse anti-APC (Ab-7, clone CC-1, Calbiochem OP80), mouse anti-ubiquitin (Enzo Life Sciences BML-PW8810), rabbit anti-RAB5 (LifeSpan Biosciences LS-C138527), guinea pig anti-p62 (American Research Products 03-GP62-C), mouse anti-myelin basic protein (MBP) (Covance SMI99), goat anti-SOX10 (Santa Cruz sc-17342X), mouse anti-RAB11 (Transduction Laboratories R56320), mouse anti-EEA1 (Abcam ab15846), rabbit anti-RAB7 (Sigma R4779), mouse anti-RAB7 (Abcam 58029) and mouse anti-NeuN (clone:A60, MilliPore MAB377). Immunolabelling was detected using fluorescent secondary antibodies (Vector Labs) or horseradish peroxidase (HRP)-conjugated secondary antibodies or HRP-conjugated avidin and biotinylated secondary antibodies of the appropriate isotype (Vector Labs) and the substrates diaminobenzidine (Trevigen), Vector Blue (Vector Labs) and/or NovaRed (Vector Labs). Most sections processed using enzymatic methods were counterstained with hematoxylin. Luxol fast blue staining was performed following standard protocols. For all studies, experimental and control samples were processed together to eliminate inter-experimental variability. Stained sections were imaged on an AxioImagerM1 microscope (Zeiss) using an A623C colour camera (Pixielink). Fluorescently

stained sections were imaged on a Fluoview 1000 confocal microscope (Olympus).

Statistics

Body weight and TSG101 immunoblot band intensity data were assessed for statistically significant differences using Student's *t*-test.

Author contribution

W.P.W. and T.M.G. conceived of all the experiments, performed most of them and prepared the manuscript. A.O. generated brain sections from RML-inoculated mice. A.L.E. and K.Y.W. created the *Rab7* and *Tsg101* conditional knockout mice, respectively. All authors reviewed and approved the final version of the manuscript.

Funding

This work was funded by The McLaughlin Research Institute and its generous supporters. W.P.W. was supported by the Oakland family and the Montana Department of Commerce.

Acknowledgements

We are grateful to Sarah Anderson and Derek Silvius for technical assistance, Anita Pecukonis and Rachel Marden for animal care, and Drs. Misol Ahn and Stephen DeArmond for sharing RML-inoculated brain specimens.

Conflict of interest statement

The authors have declared no conflict of interest.

References

Arellano-Anaya, Z.E., Huor, A., Leblanc, P., Lehmann, S., Provansal, M., Raposo, G., Andreoletti, O. and Vilette, D. (2015) Prion strains are differentially released through the exosomal pathway. Cell. Mol. Life. Sci. **72**, 1185–1196

Artigas, J., Niedobitek, F., Grosse, G., Heise, W. and Gosztonyi, G. (1989) Spongiform encephalopathy in AIDS dementia complex: report of five cases. J. Acquir. Immune. Defic. Syndr. **2**, 374–381

Baron, W., Ozgen, H., Klunder, B., de Jonge, J.C., Nomden, A., Plat, A., Trifilieff, E., de Vries, H. and Hoekstra, D. (2015) The major myelin-resident protein PLP is transported to myelin membranes via a transcytotic mechanism: involvement of sulfatide. Mol. Cell. Biol. **35**, 288–302

Beck, E., Daniel, P.M., Davey, A.J., Gajdusek, D.C. and Gibbs, C.J., Jr. (1982) The pathogenesis of transmissible spongiform encephalopathy: an ultrastructural study. Brain **105** (**Pt 4**), 755–786

Bleck, M., Itano, M.S., Johnson, D.S., Thomas, V.K., North, A.J., Bieniasz, P.D. and Simon, S.M. (2014) Temporal and spatial organization of ESCRT protein recruitment during HIV-1 budding. Proc. Natl. Acad. Sci. U.S.A. **111**, 12211–12216

Brown, G.K. and Squier, M.V. (1996) Neuropathology and pathogenesis of mitochondrial diseases. J. Inherit. Metab. Dis. **19**, 553–572

Budka, H. (2003) Neuropathology of prion diseases. Br. Med. Bull. **66**, 121–130

Chen, G., Zhang, Z., Wei, Z., Cheng, Q., Li, X., Li, W., Duan, S. and Gu, X. (2012) Lysosomal exocytosis in Schwann cells contributes to axon remyelination. Glia **60**, 295–305

Chow, C.Y., Zhang, Y., Dowling, J.J., Jin, N., Adamska, M., Shiga, K., Szigeti, K., Shy, M.E., Li, J., Zhang, X., Lupski, J.R., Weisman, L.S. and Meisler, M.H. (2007) Mutation of FIG4 causes neurodegeneration in the pale tremor mouse and patients with CMT4J. Nature **448**, 68–72

Clayton, E.L., Mizielinska, S., Edgar, J.R., Nielsen, T.T., Marshall, S., Norona, F.E., Robbins, M., Damirji, H., Holm, I.E., Johannsen, P., Nielsen, J.E., Asante, E.A., Collinge, J. and Isaacs, A.M. (2015) Frontotemporal dementia caused by CHMP2B mutation is characterised by neuronal lysosomal storage pathology. Acta. Neuropathol **130**, 511–523

Doerflinger, N.H., Macklin, W.B. and Popko, B. (2003) Inducible site-specific recombination in myelinating cells. Genesis **35**, 63–72

Doyotte, A., Russell, M.R., Hopkins, C.R. and Woodman, P.G. (2005) Depletion of TSG101 forms a mammalian "Class E" compartment: a multicisternal early endosome with multiple sorting defects. J. Cell. Sci. **118**, 3003–3017

Erdmann, G., Schutz, G. and Berger, S. (2007) Inducible gene inactivation in neurons of the adult mouse forebrain. BMC Neurosci. **8**, 63

Ersdal, C., Goodsir, C.M., Simmons, M.M., McGovern, G. and Jeffrey, M. (2009) Abnormal prion protein is associated with changes of plasma membranes and endocytosis in bovine spongiform encephalopathy (BSE)-affected cattle brains. Neuropathol. Appl. Neurobiol. **35**, 259–271

Feldmann, A., Amphornrat, J., Schonherr, M., Winterstein, C., Mobius, W., Ruhwedel, T., Danglot, L., Nave, K.A., Galli, T., Bruns, D., Trotter, J. and Kramer-Albers, E.M. (2011) Transport of the major myelin proteolipid protein is directed by VAMP3 and VAMP7. J. Neurosci. **31**, 5659–5672

Fevrier, B., Vilette, D., Archer, F., Loew, D., Faigle, W., Vidal, M., Laude, H. and Raposo, G. (2004) Cells release prions in association with exosomes. Proc. Natl. Acad. Sci. U.S.A. **101**, 9683–9688

Gomez-Lucia, E. (2005) The other transmissible spongiform encephalopathies. Rev. Neurosci. **16**, 159–179

Goudreau, G., Carpenter, S., Beaulieu, N. and Jolicoeur, P. (1996) Vacuolar myelopathy in transgenic mice expressing human immunodeficiency virus type 1 proteins under the regulation of the myelin basic protein gene promoter. Nat. Med. **2**, 655–661

He, L., Lu, X.Y., Jolly, A.F., Eldridge, A.G., Watson, S.J., Jackson, P.K., Barsh, G.S. and Gunn, T.M. (2003) Spongiform degeneration in mahoganoid mutant mice. Science **299**, 710–712

Heiseke, A., Aguib, Y. and Schatzl, H.M. (2010) Autophagy, prion infection and their mutual interactions. Curr. Issues. Mol. Biol. **12**, 87–97

Henne, W.M., Buchkovich, N.J. and Emr, S.D. (2011) The ESCRT pathway. Dev. Cell **21**, 77–91

Holm, I.E., Englund, E., Mackenzie, I.R., Johannsen, P. and Isaacs, A.M. (2007) A reassessment of the neuropathology of frontotemporal dementia linked to chromosome 3. J. Neuropathol. Exp. Neurol. **66**, 884–891

Jiao, J., Kim, H.Y., Liu, R.R., Hogan, C.A., Sun, K., Tam, L.M. and Gunn, T.M. (2009a) Transgenic analysis of the physiological functions of mahogunin ring finger-1 isoforms. Genesis **47**, 524–534

Jiao, J., Sun, K., Walker, W.P., Bagher, P., Cota, C.D. and Gunn, T.M. (2009) Abnormal regulation of TSG101 in mice with spongiform neurodegeneration. Biochim. Biophys. Acta. **1792**, 1027–1035

Jin, N., Chow, C.Y., Liu, L., Zolov, S.N., Bronson, R., Davisson, M., Petersen, J.L., Zhang, Y., Park, S., Duex, J.E., Goldowitz, D., Meisler, M.H. and Weisman, L.S. (2008) VAC14 nucleates a protein complex essential for the acute interconversion of PI3P and PI(3,5)P(2) in yeast and mouse. EMBO J. **27**, 3221–3234

Kim, B.Y., Olzmann, J.A., Barsh, G.S., Chin, L.S., and Li, L. (2007) Spongiform neurodegeneration-associated E3 ligase mahogunin ubiquitylates TSG101 and regulates endosomal trafficking. Mol. Biol. Cell **18**, 1129–1142

Kovacs, G.G., Gelpi, E., Strobel, T., Ricken, G., Nyengaard, J.R., Bernheimer, H. and Budka, H. (2007) Involvement of the endosomal-lysosomal system correlates with regional pathology in Creutzfeldt–Jakob disease. J. Neuropathol. Exp. Neurol. **66**, 628–636

Kovacs, G.G., Molnar, K., Keller, E., Botond, G., Budka, H. and Laszlo, L. (2012) Intraneuronal immunoreactivity for the prion protein distinguishes a subset of E200K genetic from sporadic Creutzfeldt–Jakob disease. J. Neuropathol. Exp. Neurol. **71**, 223–232

Kramer-Albers, E.M., Bretz, N., Tenzer, S., Winterstein, C., Mobius, W., Berger, H., Nave, K.A., Schild, H. and Trotter, J. (2007) Oligodendrocytes secrete exosomes containing major myelin and stress-protective proteins: trophic support for axons? Proteomics. Clin. Appl. **1**, 1446–1461

Krasniak, C.S. and Ahmad, S.T. (2016) The role of CHMP2B in autophagy and frontotemporal dementia. Brain Res. doi:10.1016/j.brainres.2016.02.051

Kumar, S., Mattan, N.S. and de Vellis, J. (2006) Canavan disease: a white matter disorder. Ment. Retard. Dev. Disabil. Res. Rev. **12**, 157–165

Kuo, S.M., Wang, L.Y., Yu, S., Campbell, C.E., Valiyaparambil, S.A., Rance, M. and Blumenthal, K.M. (2013) The N-terminal basolateral targeting signal unlikely acts alone in the differential trafficking of membrane transporters in MDCK cells. Biochemistry **52**, 5103–5116

Lee, J.A. and Gao, F.B. (2009) Inhibition of autophagy induction delays neuronal cell loss caused by dysfunctional ESCRT-III in frontotemporal dementia. J. Neurosci. **29**, 8506–8511

Lee, J.A. and Gao, F.B. (2012) Neuronal functions of ESCRTs. Exp. Neurobiol. **21**, 9–15

Liberski, P.P. (2004) Spongiform change—an electron microscopic view. Folia. Neuropathol. **42(Suppl B)**, 59–70

Mancardi, G.L., Mandybur, T.I. and Liwnicz, B.H. (1982) Spongiform-like changes in Alzheimer's disease. An ultrastructural study. Acta. Neuropathol. **56**, 146–150

Martinez, A.J., Sell, M., Mitrovics, T., Stoltenburg-Didinger, G., Iglesias-Rozas, J.R., Giraldo-Velasquez, M.A., Gosztonyi, G., Schneider, V., Cervos-Navarro, J. (1995) The neuropathology and epidemiology of AIDS. A Berlin experience. A review of 200 cases. Pathol. Res. Pract. **191**, 427–443

Masters, C.L. and Richardson, E.P., Jr. (1978) Subacute spongiform encephalopathy (Creutzfeldt–Jakob disease). The nature and progression of spongiform change. Brain **101**, 333–344

Mazze, F.M. and Degreve, L. (2006) The role of viral and cellular proteins in the budding of human immunodeficiency virus. Acta Virol. **50**, 75–85

Parkinson, N., Ince, P.G., Smith, M.O., Highley, R., Skibinski, G., Andersen, P.M., Morrison, K.E., Pall, H.S., Hardiman, O., Collinge, J., Shaw, P.J. and Fisher, E.M. (2006) ALS phenotypes with mutations in CHMP2B (charged multivesicular body protein 2B). Neurology **67**, 1074–1077

Razi, M. and Futter, C.E. (2006) Distinct roles for Tsg101 and Hrs in multivesicular body formation and inward vesiculation. Mol. Biol. Cell **17**, 3469–3483

Roy, S.G., Stevens, M.W., So, L. and Edinger, A.L. (2013) Reciprocal effects of rab7 deletion in activated and neglected T cells. Autophagy **9**, 1009–1023

Shacka, J.J., Roth, K.A. and Zhang, J. (2008) The autophagy-lysosomal degradation pathway: role in neurodegenerative disease and therapy. Front. Biosci. **13**, 718–736

Silvius, D., Pitstick, R., Ahn, M., Meishery, D., Oehler, A., Barsh, G.S., DeArmond, S.J., Carlson, G.A. and Gunn, T.M. (2013) Levels of the mahogunin ring finger 1 E3 ubiquitin ligase do not influence prion disease. PLoS One **8**, e55575

Simons, M., Kramer, E.M., Macchi, P., Rathke-Hartlieb, S., Trotter, J., Nave, K.A. and Schulz, J.B. (2002) Overexpression of the myelin proteolipid protein leads to accumulation of cholesterol and proteolipid protein in endosomes/lysosomes: implications for Pelizaeus–Merzbacher disease. J. Cell Biol. **157**, 327–336

Skibinski, G., Parkinson, N.J., Brown, J.M., Chakrabarti, L., Lloyd, S.L., Hummerich, H., Nielsen, J.E., Hodges, J.R., Spillantini, M.G., Thusgaard, T., Brandner, S., Brun, A., Rossor, M.N., Gade, A., Johannsen, P., Sorensen, S.A., Gydesen, S., Fisher, E.M. and Collinge, J. (2005) Mutations in the endosomal ESCRTIII-complex subunit CHMP2B in frontotemporal dementia. Nat. Genet. **37**, 806–808

Smith, T.W., Anwer, U., DeGirolami, U. and Drachman, D.A. (1987) Vacuolar change in Alzheimer's disease. Arch. Neurol. **44**, 1225–1228

Soriano, P. (1999) Generalized lacZ expression with the ROSA26 Cre reporter strain. Nat. Genet. **21**, 70–71

Stendel, C., Roos, A., Kleine, H., Arnaud, E., Ozcelik, M., Sidiropoulos, P.N., Zenker, J., Schupfer, F., Lehmann, U., Sobota, R.M., Litchfield, D.W., Luscher, B., Chrast, R., Suter, U. and Senderek, J. (2010) SH3TC2, a protein mutant in Charcot–Marie–Tooth neuropathy, links peripheral nerve myelination to endosomal recycling. Brain **133**, 2462–2474

Sun, K., Johnson, B.S. and Gunn, T.M. (2007) Mitochondrial dysfunction precedes neurodegeneration in mahogunin (Mgrn1) mutant mice. Neurobiol. Aging **28**, 1840–1852

Trajkovic, K., Dhaunchak, A.S., Goncalves, J.T., Wenzel, D., Schneider, A., Bunt, G., Nave, K.A. and Simons, M. (2006) Neuron to glia signaling triggers myelin membrane exocytosis from endosomal storage sites. J. Cell Biol. **172**, 937–948

Traka, M., Podojil, J.R., McCarthy, D.P., Miller, S.D. and Popko, B. (2016) Oligodendrocyte death results in immune-mediated CNS demyelination. Nat. Neurosci. **19**, 65–74

Urwin, H., Authier, A., Nielsen, J.E., Metcalf, D., Powell, C., Froud, K., Malcolm, D.S., Holm, I., Johannsen, P., Brown, J., Fisher, E.M., van der Zee, J., Bruyland, M., Van Broeckhoven, C., Collinge, J., Brandner, S., Futter, C. and Isaacs, A.M. (2010) Disruption of endocytic trafficking in frontotemporal dementia with CHMP2B mutations. Hum. Mol. Genet. **19**, 2228–2238

Valiathan, R.R. and Resh, M.D. (2004) Expression of human immunodeficiency virus type 1 gag modulates ligand-induced downregulation of EGF receptor. J. Virol. **78**, 12386–12394

van der Zee, J., Urwin, H., Engelborghs, S., Bruyland, M., Vandenberghe, R., Dermaut, B., De Pooter, T., Peeters, K., Santens, P., De Deyn, P.P., Fisher, E.M., Collinge, J., Isaacs, A.M. and Van Broeckhoven, C. (2008) CHMP2B C-truncating mutations in frontotemporal lobar degeneration are associated with an aberrant endosomal phenotype in vitro. Hum. Mol. Genet. **17**, 313–322

Vanlandingham, P.A. and Ceresa, B.P. (2009) Rab7 regulates late endocytic trafficking downstream of multivesicular body biogenesis and cargo sequestration. J. Biol. Chem. **284**, 12110–12124

Wagner, K.U., Krempler, A., Qi, Y., Park, K., Henry, M.D., Triplett, A.A., Riedlinger, G., Rucker, I.E. and Hennighausen, L. (2003) Tsg101 is essential for cell growth, proliferation, and cell survival of embryonic and adult tissues. Mol. Cell. Biol. **23**, 150–162

Wang, D., Chan, C.C., Cherry, S. and Hiesinger, P.R. (2013) Membrane trafficking in neuronal maintenance and degeneration. Cell. Mol. Life. Sci. **70**, 2919–2934

Watson, J.A., Bhattacharyya, B.J., Vaden, J.H., Wilson, J.A., Icyuz, M., Howard, A.D., Phillips, E., DeSilva, T.M., Siegal, G.P., Bean, A.J., King, G.D., Phillips, S.E., Miller, R.J. and Wilson, S.M. (2015) Motor and sensory deficits in the teetering mice result from mutation of the ESCRT component HGS. PLoS Genet. **11**, e1005290

Wells, G.A. and Wells, M. (1989) Neuropil vacuolation in brain: a reproducible histological processing artefact. J. Comp. Pathol. **101**, 355–362

Winterstein, C., Trotter, J., Kramer-Albers, E.M. (2008) Distinct endocytic recycling of myelin proteins promotes oligodendroglial membrane remodeling. J. Cell Sci. **121**, 834–842

Zhang, Y., Zolov, S.N., Chow, C.Y., Slutsky, S.G., Richardson, S.C., Piper, R.C., Yang, B., Nau, J.J., Westrick, R.J., Morrison, S.J., Meisler, M.H. and Weisman, L.S. (2007) Loss of Vac14, a regulator of the signaling lipid phosphatidylinositol 3,5-bisphosphate, results in neurodegeneration in mice. Proc. Natl. Acad. Sci. U.S.A. **104**, 17518–17523

Zivony-Elboum, Y., Westbroek, W., Kfir, N., Savitzki, D., Shoval, Y., Bloom, A., Rod, R., Khayat, M., Gross, B., Samri, W., Cohen, H., Sonkin, V., Freidman, T., Geiger, D., Fattal-Valevski, A., Anikster, Y., Waters, A.M., Kleta, R., Falik-Zaccai, T.C. (2012) A founder mutation in Vps37A causes autosomal recessive complex hereditary spastic paraparesis. J. Med. Genet. **49**, 462–472

Zolov, S.N., Bridges, D., Zhang, Y., Lee, W.W., Riehle, E., Verma, R., Lenk, G.M., Converso-Baran, K., Weide, T., Albin, R.L., Saltiel, A.R., Meisler, M.H., Russell, M.W. and Weisman, L.S. (2012) In vivo, Pikfyve generates PI(3,5)P2, which serves as both a signaling lipid and the major precursor for PI5P. Proc. Natl. Acad. Sci. U.S.A. **109**, 17472–17477

Received: 14 March 2016; Revised: 5 July 2016; Accepted: 6 July 2016; Accepted article online: 13 July 2016